Hydrogeology Journal (2022) 30:2459–2477
https://doi.org/10.1007/s10040-022-02562-w

REPORT

Natural occurrence and controls of arsenic in groundwater in a semiarid basin in the Mexican Altiplano

Dario Cauich-Kau[1,2] · Thomas R. Rüde[1] · Antonio Cardona-Benavides[2] · Javier Castro-Larragoitia[2]

Received: 14 August 2021 / Accepted: 21 October 2022 / Published online: 14 November 2022

Abstract

The sources, mobility, and controlling processes of arsenic (As) in an aquifer system in the Cerritos-Guadalcazar area of Central Mexico were investigated. High As concentrations (up to 128 µg/L) in groundwater were found to be associated with both primary sources (rocks and tailings) and secondary sources (soil and sediments). The high As concentrations in the otherwise pristine Cerritos shallow granular aquifer are the result of a distant source of As-rich sediments eroded from a mineralized area in the recharge zone of a karstic aquifer. An intermediate groundwater flow system delivers the As load from the karstic to the granular aquifer. In addition, identification of a Na–Cl water type in the shallow granular aquifer indicates a regional flow; however, additional information is needed to corroborate this assumption. Local flows in the karstic aquifer are Ca–HCO_3 water type with low (<1 µg/L) dissolved As concentrations. Principle axis factor analysis shows distinct groupings associated with different aquifer characteristics. The sulfate factor dominates in the southern area of the granular aquifer, which explains 30% of the total variance. The arsenic-uranium factor is expressed in samples from deep and dug wells tapping the basin sediments. A conceptual model was developed where the path of the As is shown. Three groups of samples showed negative correlation among deuterium excess and As concentrations. Evaporation modeling to simulate the As enrichment showed that evaporation processes play an important role in As behavior. This research can provide a tool for further studies in the Sierra Madre Oriental.

Keywords Arsenic · Arid regions · Groundwater monitoring · Hydrochemistry · Mexico

Introduction

Arsenic (As) is an inorganic trace element naturally occurring in water. The incidence of As concentrations above drinking water standards in groundwater is a threat to human health (He et al. 2020, 2021; Podgorski and Berg 2020). Naturally occurring in rocks, soils, water, and air, As is mainly associated with sulfide minerals or hydroxides (Bundschuh et al. 2012; Chakrabarti et al. 2018; Guo et al. 2014; Srivastava and Kumar Sharma 2013). Most of the investigations of dissolved As have evaluated primary As sources such as sulfides, oxides, phosphates, silicates, and sulphate minerals, volcanic glass, and hydrothermal minerals, such as orpiment (As_2S_3) and realgar (AsS; e.g Smedley and Kinniburgh 2013; Wang et al. 2019; Zabala et al. 2016). Also secondary sources such as Fe-, Mn-, and Al-(hydr) oxides and clays have been considered (e.g. Nicolli et al. 2012; Panagiotaras and Nikolopoulos 2015; Zhu et al. 2015). Common As-bearing minerals occurring as the source of this element in groundwater are pyrite (FeS_2) and arsenopyrite (FeAsS; e.g. Sorg et al. 2014; Wei et al. 2021), and in many cases, As can co-occur with other elements such as fluoride, iodine, and iron (Li et al. 2021). The reactivity and mobility of As are controlled by Fe minerals and the prevailing physicochemical conditions (pH, redox potential, ionic strength, and organic matter content). The As concentration in groundwater depends on several factors such as the geological and tectonic setting, the hydrogeological regime, and groundwater exploitation.

Naturally occurring As as a pollutant in groundwater has been identified in many areas worldwide, including Western USA, Central America, South America, South and Southeast

✉ Dario Cauich-Kau
dario.cauich@rwth-aachen.de

[1] Institute of Hydrogeology, RWTH Aachen University, Lochnerstr. 4-20, 52064 Aachen, Germany

[2] Engineering Faculty, Earth Science Department, Universidad Autónoma de San Luis Potosí, Dr. Manuel Nava No. 8, 78290 San Luis Potosí, Mexico

Asia, New Zealand, Germany, Iceland, and Norway (e.g. Ahmed et al. 2004; Alarcón-Herrera et al. 2020; Bundschuh et al. 2012; Bundschuh et al. 2012; Guo et al. 2011, 2012; López et al. 2012; Nicolli et al. 2010; Biswas et al. 2011; Rüde 1996). South and Southeast Asia are a typically high As regions where over 100 million people have been exposed to As-contaminated groundwater (e.g. Guo et al. 2012, 2011; Meng et al. 2017).

In the early 1960s, Mexican institutions reported health problems for inhabitants in arid to semiarid areas, because of the consumption of groundwater with high As concentrations (e.g. Alarcón-Herrera et al. 2013; Banning et al. 2012; Morales et al. 2015; Navarro et al. 2017). Two main As sources have been identified in Mexico: anthropogenic and geogenic. The former is due to mining and metallurgical activities and the latter is because of the specific physicochemical conditions (sulfide oxidation, climatic conditions, and low pH). Most of the population affected by these conditions live in rural areas where their main economic activities are seasonal agriculture and cattle ranching, and where groundwater rich in dissolved As is consumed from shallow aquifers.

Recently, elevated groundwater As concentrations (up to 128 µg/L) were reported in the central part of San Luis Potosi (SLP) State, in Central Mexico, particularly in the Guadalcazar area and Cerritos Basin (CB; Konefke 2018; Palm 2008). At this point, the As concentrations were identified not only in rocks in the mineralized (Guadalcazar) area upstream of the CB, but also in the shallow groundwater of the basin fill sediments. Regarding As described in the preceding, most of the reviewed scientific papers describe either primary or secondary As sources to groundwater. It is important to evaluate alternative scenarios of dissolved As load contributed from primary and secondary sources to groundwater flow systems, and when additional physical processes modify groundwater composition. Therefore, this report aims to provide a deeper understanding of: (1) As concentrations in primary and secondary sources; (2) the link between the primary and secondary As sources to groundwater of the Guadalcazar area and the CB; (3) the spatial As distribution; and (4) identification of factors controlling the As mobility in the shallow aquifers.

Materials and methods

Study area

The study area, with a surface area of 1,350 km^2, lies on the Sierra Madre Oriental (SMO) in central Mexico, bounded to the north by the Guadalcazar mountains−1,800 meters above sea level (masl)—and to the west and east by ranges of folded limestone. The CB is oriented NW–SE, and is controlled by the SMO regional trend; it slopes from NW–SE, and the average plain elevation is 1,130 masl (1,160–1,100 masl). The area is situated between latitude 22°05′ and 22°45′N and longitude 100°30′ to 100°05′W (geographic coordinates; Fig. 1) and includes the municipalities of Cerritos, Guadalcazar, and Villa Juarez, with a total population of 57,500 inhabitants, where agriculture and livestock are the main economic activities (INEGI 2020). Especially at the southern end of the study area, the development of greenhouse vegetable production has added an important stress factor to the natural resources of the area. The climate is semiarid, with an annual average precipitation of 620 mm in the northwest and 660 mm in the southeast with potential evapotranspiration in the region of 2,369–1,838 mm for the period 1962–2017 (CONAGUA 2019). The rainy season lasts from May to October. Annual average air temperature in the area ranges from 18 °C (average monthly range from 13 to 21 °C) to 20 °C in Cerritos (average monthly range from 14 to 24 °C). Thermal variation from the rainy to the dry season is 9 °C, with the moisture source originating from the Gulf of Mexico (Calva 2011). The area is located within the Panuco Hydrogeological Region (No. 26). Ephemeral and intermittent streams are recognized in the northern part of the area; from direct field observations, it was identified that a fraction of the surface flow infiltrates the CB plain. In addition, there is a perennial stream fed by several springs located to the south of the study area discharging to the neighboring basin. Guadalcazar is located in a large polje and during the rainy season, surface water is ponded at the southern edge of the polje.

The study area includes two main important aspects with respect to this study: (1) gypsum rocks outcropping in the mountains and the sediments of a former lake dominating the geology of the CB, and (2) large-scale Cretaceous karstification resulting the Guadalcazar Polje (GP). There, a granitic intrusion produced an ore body (see the following) in the Tertiary, which was mined for Au and Ag in the past at the site of El Realejo (ER). The Valles–San Luis platform of Mesozoic age is one of the five carbonate rock provinces in Mexico and consists of folded sedimentary marine rocks including evaporites, limestone, sandstone, and shales (Rodríguez-Hernández et al. 2009; Tristán-González 1977). From the end of the Jurassic and continuing through the lower Cretaceous, the Guaxcama Formation (Gypsum-Anhydrite, Fig. 1) of Aptian age was deposited. These evaporitic rocks outcrop to the south of Villa Juarez. The sequence is constituted predominantly by light- to dark-gray anhydrite layers (2–50 cm thick), with some interbedded white gypsum and dark gray dolomite. The Rioverde borehole (40 km southeast of Villa Juarez) encountered this formation from the land surface up to a depth of 3,000 m (Torres-Hernandez 1994). Sediments of Albian-Cenomanian age comprise the Abra Formation (Limestone, Fig. 1), consisting of tightly folded

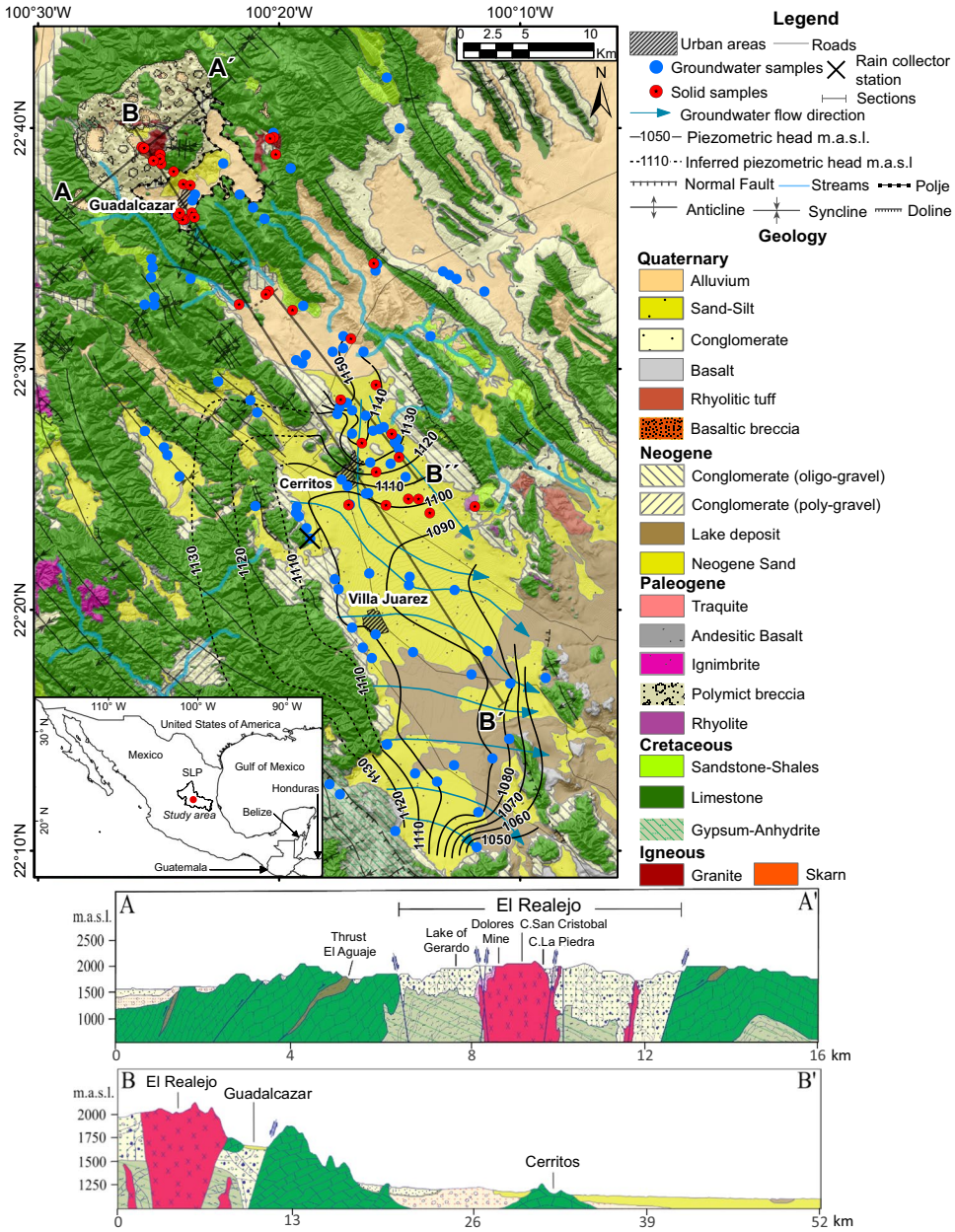

Fig. 1 Study area location, general geology, sections A–A′ and B–B′, and general groundwater flow direction (modified from Servicio Geológico Mexicano (SGM 1998, 2000, 2008, 2010). Legend: SLP State of San Luis Potosi

carbonate marine rocks with a NW–SE trend outcropping in the mountain ranges of the area and concordantly overlying the Gypsum-Anhydrite sequence. It is a light-brown to gray fine-grained limestone (ranging from mudstone to wackestone and grainstone) with dark-brown dolomite horizons, 0.8–2.6-m-thick layers, occasionally massive. Corrosion and karstification have taken place at different scales. The largest feature is the GP which is a closed basin with a flat bottom and steep peripheral slopes. Except for some intermittent streams, drainage is mostly underground and sinkholes at the southern rim of the polje mark the inflow of surface water to the karst aquifer.

Felsic rocks of Tertiary age intruded the calcareous sequence; magmatic activity took place forming a mineralized granite in the northwest ER area with some felsic volcanic rocks to the east (Chryssoulis and Wilkinson 1983; Fig. 1). Furthermore, during the subsequent tectonic extension, the CB developed as one of several NW–SE striking basins (Soto Araiza et al. 2007).

Two types of structures characterize the study area, the first related to the Laramide Orogeny and the second related to the karstification processes. The anticlines of the Sierra de Guadalcazar to the northwest of CB are an example of the former. Aligned with this orogeny are several ductile to ductile-brittle tectonic features like foliation planes in the hinge zone of anticlines and synclines of the Gypsum-Anhydrite and Sandstone-Shales Formations showing a NW–SE orientation, which implies an E–NE orientated

stress (Soto Araiza et al. 2007). The Sierra de Guadalcazar is a major structure formed during the Laramide Orogeny (Torres-Hernández 1994). Additionally, a later extensional regime led to mainly brittle deformation and had two different phases. The first formed NW–SE discontinuities such as the Cerritos-Villa Juarez Valley, while the second phase produced NE–SW-orientated faults and corresponding volcanism (Torres-Hernández 1994).

Gypsum diapirism started the development of the GP (Torres-Hernández 1994). The weakening of the covering folded limestone units enabled deep karstification and polje formation during the lower Tertiary age. Granitic magma intruded the center of the collapsed area in the Oligocene and the ore body formed at this or slightly later stage (Torres-Hernández 1994). Successive erosion led to the current shape of the GP. The topography and relief control the general groundwater flow direction to the southeast (Fig. 1). The recharge comes from the sierras located to the northeast and northwest as well as by surface runoff, recharge induced by irrigation returns, leaks in the water irrigation systems, and leaks in drinking-water distribution systems. The total average annual recharge received by the aquifer corresponds to the sum of all the volumes entering the aquifer. In this case, its value is ca. 72.7 hm^3/year. Discharge from the aquifer occurs mainly by pumping, in a limited region by horizontal subsurface flow, and springs; therefore, the discharge volume is about 50.4 hm^3/year.

The Gypsum-Anhydrite formation constitutes the regional hydrogeological basement for the groundwater flow systems. In addition, Sandstone-Shales units in the folded rock pile provoke changes from unconfined to confined behavior of the hard rock aquifer. INEGI (2002) identifies two different aquifers; the first is a karst aquifer of folded calcareous limestones, which allows a regional flow through the karstic system. This aquifer is unconfined and consists of limestones and extrusive igneous rocks; hydraulic conductivity is assumed as 1×10^{-4} m/s. However, four pumping tests were performed at the deep wells 14-16, 14-57, 14-80, and 14-107, giving hydraulic conductivity ranging from 8.8×10^{-7} to 4.2×10^{-6}. Likewise, the formation of synclines and anticlines enables a hydrological connection between the limestone and the conglomerates and alluvium located at the top of the sequence. The second heterogeneous aquifer consists of alluvial sediments and is located in the center of CB. To the south and southeast, this aquifer consists of a Quaternary gypsum unit and conglomerates in the lateral borders. While the fine granular material shows a low permeability, the western parts consist of calcareous conglomerates with higher permeability. At a depth of ca. 300 m, the aquifer changes from unconfined in the northwest to confined at the south and east of the village of Villa Juarez.

The water quality differs from low salinity (minimum electrical conductivity, EC = 180 µS/cm) to high salinity (maximum EC = 4,770 µS/cm). The highest salinities occur in the southern to southeastern parts, where the groundwater circulates through gypsum sediments, while low salinities occur to the north, northwest, and west of Cerritos, where the water is in contact with the calcareous units. The groundwater levels range between 2.5 and 34 m below surface. Some dug wells dry out from time to time due to the lack of sufficient recharge during rainy season. Water supply to the entire population of the study area depends on the groundwater resources. On the one hand, deep wells (30–180 m depth) tapping the limestones are the main source of water supply in the city of Cerritos (hereafter Cerritos). In contrast, dug wells (5–15 m depth) tapping the basin fill are the main source for water supply for cattle ranching, agriculture irrigation, and water supply to the rural communities surrounding Cerritos. Further, in the Guadalcazar area, springs, dug wells, and deep wells are the main groundwater sources tapping the limestone units. Due to the lack of a treatment structure, sewage systems discharge their untreated wastewater directly to dolines with the risk of polluting the groundwater. For this semiarid region, it is important to have a good management of the resource in order to provide good quality drinking water to householders.

Groundwater sampling

Field trips have identified a total of 65 deep wells, 85 dug wells, 25 springs, and several ponds in the study area. With this information, a representative set of water samples for chemical and isotope analysis from the karstic and granular aquifers was collected (Palm 2008). Following the preliminary interpretation of the results, specifically the identification of high As concentrations in some dug wells, additional groundwater and surface-water sampling campaigns were conducted in 2018 (Konefke 2018) and 2019. A total of 95 water samples were taken from 13 springs, 41 dug wells (5–15 m deep), 39 deep wells (30–180 m deep), 1 pond, and 1 drainage ditch (Fig. 1). Water samples were taken from deep wells penetrating the karstic aquifer and the unconfined granular aquifer, and they are screened from the phreatic level to total depth; dug wells tap the phreatic water level of the unconfined aquifer. Karstic aquifer natural discharges provide water for low-yield (<2 L/s) ephemeral springs and high-yield (>50 L/s) perennial springs. In addition, the Gypsum-Anhydrite unit hosts some springs in the southwestern part of the study area. Locations of all water samples are shown in Fig. 1, where they have been classified according to sampling site conditions. Deep and dug wells were purged prior to sampling for at least 5–10 min; however, according to water use (public, irrigation, domestic, cattle), they had been pumped continuously for several hours. Pumping equipment included submersible and vertical pumps (2–8 inches (5–20 cm) in diameter) and wind-powered piston

pumps (1–2 inches (2.5–5 cm) in diameter. Spring sampling was done by a hand-operated bailer or a plastic tube in which samples are collected by gently lowering the bailer or a plastic tube into the water column and allowing water to fill from the base upwards through a nonreturn ball valve according to local conditions.

On-site measurements

On-site measurements included temperature (*T*), electrical conductivity (EC), pH, and dissolved oxygen (DO). The deep well and dug well head works consisted of discharge mains with either valves or discharge tubes, allowing the implementation of a plastic tube connected to a closed flow-through isolation cell to prevent CO_2 degassing and atmospheric contamination, in addition to its enhanced electrode stability. Portable field equipment was calibrated daily for pH (4.0 and 7.0 buffer solutions) and DO measurements (zero oxygen calibration solution); appropriate performance of the EC electrode was controlled daily with a calibration solution. Alkalinity determination was completed by acid-base titration on filtered (0.45 µm) samples (Gran Method, 1. 6 N H_2SO_4). Aliquots for major anions (Cl^-, SO_4^{2-}, NO_3^-, F^-) were filtered in the field through a 0.45-µm membrane and were used for laboratory analysis by ion chromatography. Filtered and acidified (1% in ultrapure HNO_3) aliquots for major cations, Si and a wide range of trace elements were analyzed either by ICP-OES (inductively coupled plasma optical emission spectroscopy, Thermo Scientific Model ICAP 700) or ICP-MS (inductively coupled plasma mass spectrometry, Thermo Scientific Model ICAP 5000). Based on sample replicability, analytical precision for ion chromatography was within 3% of the concentration, with detection limits which were between 0.01 and 0.03 mg/L for undiluted samples. Accuracy was controlled by using laboratory and field duplicates of samples. Calibrations for ICP-OES and ICP-MS analysis were performed using diluted standards. Accuracy was controlled by using duplicate analyses, appropriate laboratory standards, and checking each batch using international reference standards, including NIST-1640 and SLRS-4. Additional filtered aliquots for isotope analysis (δ^2H, $\delta^{18}O$) were measured by isotope ratio mass spectrometry. The precision of measurements for stable isotopes was ±0.1‰ (VSMOW) for $\delta^{18}O$ and ±1‰ (VSMOW) for δ^2H.

Solid sampling

In order to characterize the primary and secondary As sources, 43 solid samples were taken (Figs. 1 and 2): (1) nine rock samples were obtained including the intrusive body ER, and rhyolitic rocks (with a variable alteration grade); (2) five sediment samples from 0.15-cm-thickness sections crosswise were obtained from intermittent streams downstream of the intrusive body (see Figs. 1 and 2b); (3)

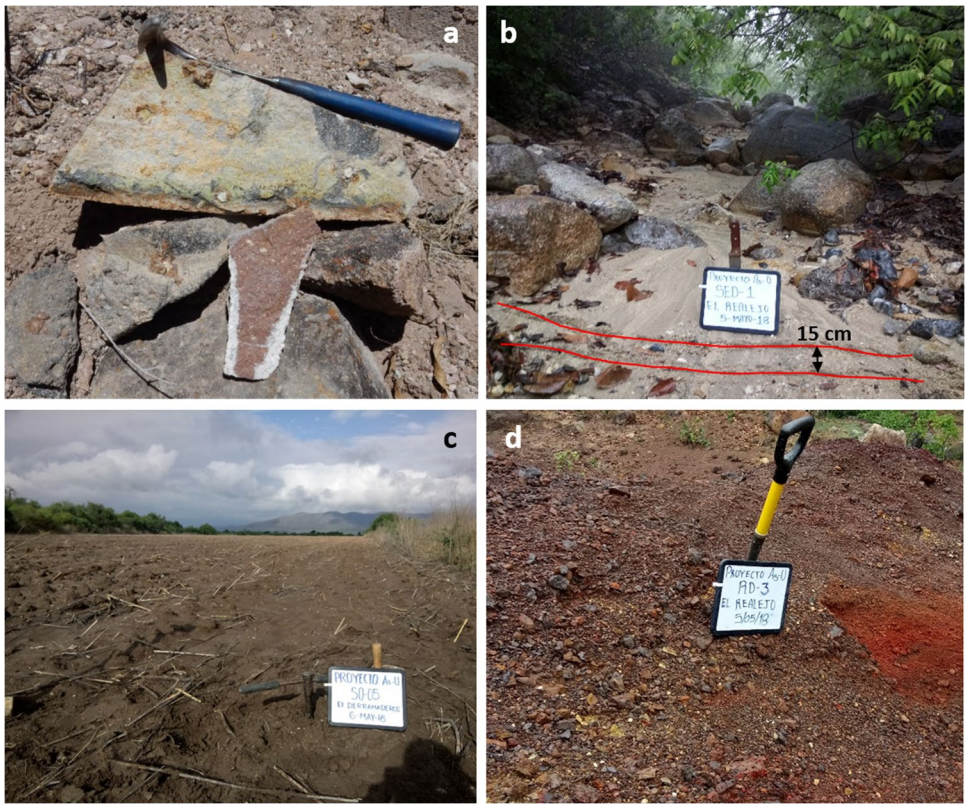

Fig. 2 Solid samples: **a** rocks, **b** sediments, **c** soils, and **d** tailings

23 soil samples were obtained in agricultural areas in order to verify the potential influence of the intrusive body and the sediments in the basin (Figs. 1 and 2c), and a handheld auger device was used for the soil sampling; and (4) 6 composite samples from selected tailings heaps were obtained at the ancient mining sites and sieved using 100 mesh (0.149 mm) screen in the field (Figs. 1 and 2c). Solid samples were dried for 5 days at room temperature and pulverized using a Retsch mechanical mortar grinder producing <10-µm-size particles. Total digestion was achieved using a microwave reaction system, adding 2 ml of ultrapure hydrofluoric (HF) and 3 ml of ultrapure nitric acid (HNO_3) to 0.1 g of sample (USEPA 2004). Digested samples were analyzed for major and trace elements using ICP-OES and ICP-MS. Accuracy was controlled using appropriate laboratory standards and checked during each batch using international reference standards, including Montana I Soil (Mackey et al. 2010) and Silver Plume granodiorite (Gunderson 1998). Results always showed a less than 10% difference from the certified value.

Data quality and statistics

In order to verify the accuracy of the groundwater results, not only duplicates and blanks were measured, but also international certified reference materials were used, and likewise for solid samples. An internal check on the analytical quality of the water chemistry results was made by the ionic balance as calculated with PHREEQC. About 77% of samples were within 5% of the ionic balance and the rest within 5 to 10%. Table 1 shows descriptive statistics of the water samples; however, Table S1 of the electronic supplementary material (ESM) shows the complete data set. For the statistics, the pond (L-01), the drainage (L-02), and one deep well (L-21) were not considered because of their extreme concentrations. The software IBM® SPSS® Statistics Version 25 was used to evaluate the data. Factor analysis was used to reduce the variables, e.g. (m) of the dataset of n samples to a few stochastically independent factors. These factors will represent certain processes that include many variables (Schafmeister 1999). Principal component analysis (PCA) has been used in many scientific publications to evaluate the correlation between the original data and each principal component. However, in this study, with a large database including random samples, PCA did not deliver useful data for further interpretation. The use of principle axis factor analysis (PAA) is appropriate because it allows a residual variance. For the calculations, a robust transformation of the data was carried

Table 1 Descriptive statistical data for field parameters, major and minor ions, and trace elements in groundwater samples. *SD* standard deviation

			Cerritos basin ($n = 92$)				
Parameter	WHO guideline	NOM-1994	Range	Average	SD	% samples above WHO guideline	% samples above NOM guideline
pH	6.5–8.5[a]	6.5–8.5	6.4–8.2	7.2	0.4	0	0
EC (µS/cm)	-	-	180–4,770	1,307	962	0	-
DO (mg/L)	-	-	0.1–10.8	4.3	2.6	-	-
T (°C)	-	-	14.9–29.9	22.6	2.8	-	-
HCO_3^- (mg/L)	250[a]	-	106–657	338	112	-	-
Cl^- (mg/L)	50	250	9.1–690	60.6	99.3	4	4
NO_3^- (mg/L)	250	-	0.4–234	24.6	37.4	11	-
SO_4^{2-} (mg/L)	200[a]	400	1–1,964	412	544	37	34
Na^+ (mg/L)	-	200	2–768	80.4	124	12	12
K^+ (mg/L)	-	-	0.6–29.1	7.6	6.1	-	-
Mg^{2+} (mg/L)	-	-	0.8–216	40	54.8	-	-
Ca^{2+} (mg/L)	-	-	32.9–589	169	123	-	-
Al (µg/L)	10	200	0.1–1,074	53.5	124	-	4
As (µg/L)	2,400	25	0.01–128	19.7	25.4	45	27
B (µg/L)	1,300	-	0.2–1,455	227	340	0	-
Ba (µg/L)	-	700	2.6–957	98.5	144	0	2
Br (µg/L)	1.5	-	1.7–3,456	388	688	-	-
F (mg/L)	0.3[a]	1.5	0.01–2.2	0.8	0.6	13	13
Fe (mg/L)	-	0.3	0.2–2,664	129	375	10	10
Li (µg/L)	80	-	0.4–466	50.5	66	-	-
Mn (µg/L)	-	150	0.01–408	34.1	79.8	10	9
Sr (µg/L)	30	-	22.6–14,180	2,843	3,282	-	-
U (µg/L)	-	-	0.01–28.8	3.8	4.7	0	-

[a]No health-based guideline value, threshold or range because of acceptability aspects

out. To do so, the original concentration minus the first quartile was divided by hinge spread.

The figures and the conceptual model presented in this research have been created using the software ArcMap® and CorelDRAW®, respectively.

Results

Solid samples

The geochemical characterization of the primary and secondary sources showed that the As concentrations found in the rocks were in the range of 1.7–1,352 mg/kg (Fig. 3; Table 2), exceeding in some places global background values (1–30 mg/kg according to Kabata-Pendias 2011; Matschullat 2000). The sample with a concentration of 1,352 mg/kg (R6, Table 2) was taken from an outcrop of the pyrite-containing intrusive body of El Realejo, indicating a primary source of As. In addition, several dykes crisscross the sample place. The material of the dykes and the surrounding material show evidence of weathering with a reddish-brown color. The sample consisted of a very fine matrix quartz and feldspar phenocrys and iron hydroxides as secondary minerals. The rhyolitic samples located at the CB are also partially As-enriched (1.8–49.9 mg/kg) and can be considered as an additional As source to the sediments and soils in the basin. Whole rock As concentrations were controlled

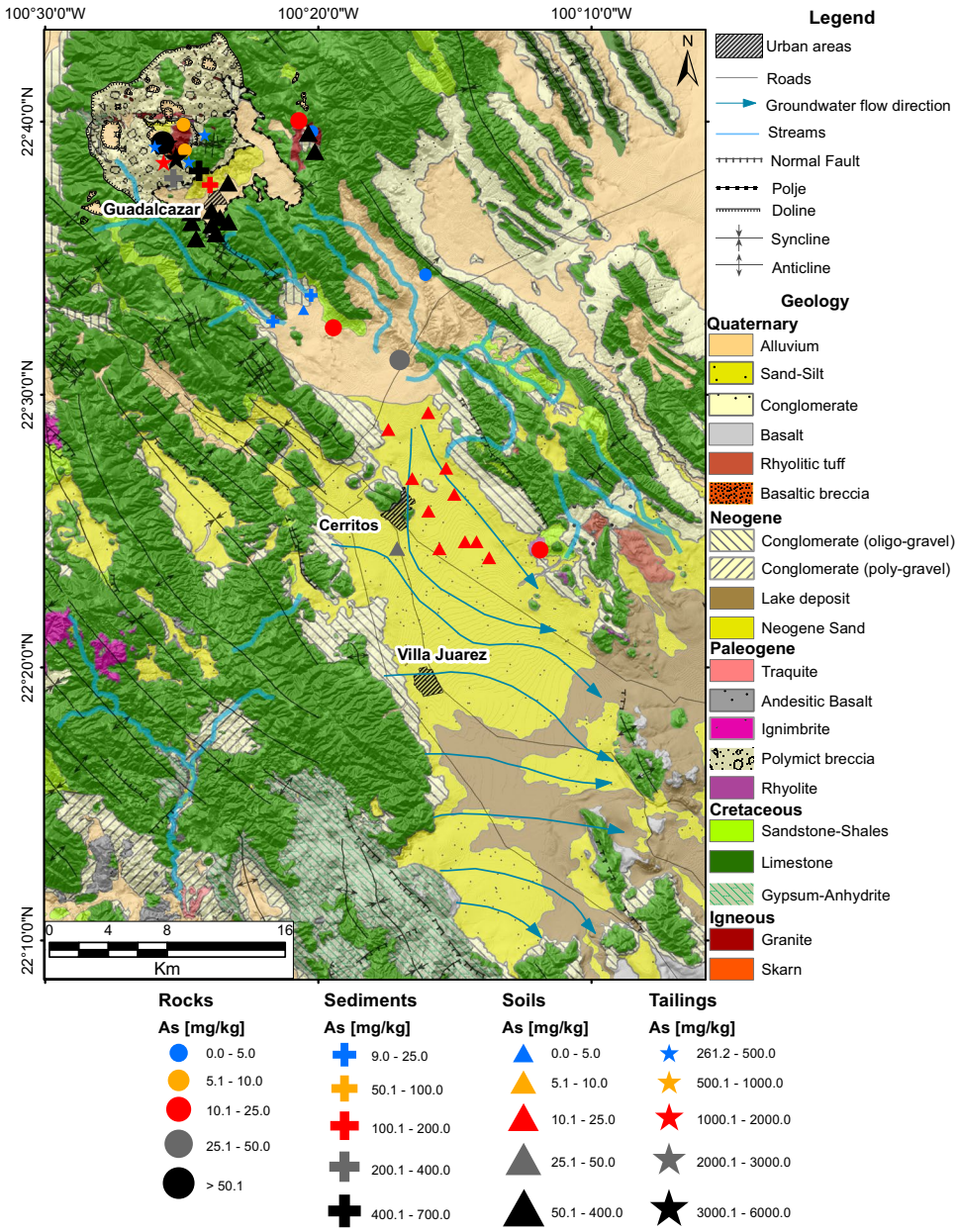

Fig. 3 Distribution and results of the solid samples

Table 2 Results for solid samples

ID	As [mg/kg]	Type	Observations
SD1	15.2	Rock	Erosive channel containing large transported rhyolitic blocks
SD2	49.9	Rock	Red colored rhyolite
C3	15.9	Rock	Outcrops at the upper part consisting of a red ignimbrite
R1	9.20	Rock	Intrusive body: taken from an outcrop near the old mining site
R2	9.57	Rock	Intrusive body: taken from an outcrop near the old mining site
R6	1,352	Rock	Intrusive body: taken from a high altered outcrop near the old mining site
RO-01	13.9	Rock	Volcanic rock with high alteration grade (Rhyolite)
RO-02	2.95	Rock	Volcanic rock (Outcrop) (Rhyolite)
RO-03	1.74	Rock	Volcanic rock (outcrop) with low alteration (Rhyolite)
SC1	9.01	Sediments	The fine material shows a brown color
SC2	16.6	Sediments	The fine material shows a brown color
R3	275	Sediments	Sample taken near the intrusive body of El Realejo
G2	152	Sediments	North of Guadalcazar. The color shows indications of oxidation and hematization
SED-1	664	Sediments	Riverbed with visible transport of intrusive material
SC3		Soil	The soil sample was taken in an agricultural field
C1	13.7	Soil	The soil sample was taken in an agricultural field
C2	18.9	Soil	The soil sample was taken in an agricultural field
C4	26.9	Soil	The soil sample was taken in an agricultural field
G1	250	Soil	Situated in the south of the Polje of Guadalcazar, close to the active doline
SO-01	337	Soil	Sample taken 3 m from the riverbed downstream body of El Realejo
SO-02	173	Soil	Sample taken near the drainage discharge at the doline
SO-03	116	Soil	The soil sample was taken in an agricultural field
SO-04	65	Soil	The soil sample was taken in an agricultural field
SO-05	10.8	Soil	The soil sample was taken in an agricultural field
SO-06	12.7	Soil	The soil sample was taken in an agricultural field
SO-07	11.4	Soil	The soil sample was taken in an agricultural field
SO-08	14.9	Soil	The soil sample was taken in an agricultural field
SO-09	14.4	Soil	The soil sample was taken in an agricultural field
SO-10	11.8	Soil	The soil sample was taken in an agricultural field
SO-11	13	Soil	The soil sample was taken in an agricultural field
SO-12	13.0	Soil	The soil sample was taken in an agricultural field
SO-13	107	Soil	The soil sample was taken in an agricultural field
SO-14	79	Soil	Sample taken at the edge of a dry riverbed
SO-15	373	Soil	Sample taken in the pond
SO-16	170	Soil	Sample taken at edge of the pond where the water does not have long contact
SO-17	306	Soil	Sample taken at the beginning of the pond
SO-18	59	Soil	Sample taken at the beginning of the calcareous hills
R4	1,340	Tailing	Taken from mining residues close to the intrusive body of Realejo
R5	391	Tailing	Taken from mining residues close to the intrusive body of Realejo
RD-1	261	Tailing	Taken from mining residues close to the intrusive body of Realejo
RD-2	326	Tailing	Taken from mining residues close to the intrusive body of Realejo
RD-3	3,078	Tailing	The color indicates oxidation, hematization, and iron hydroxides
RD-4	5,906	Tailing	The color indicates oxidation, hematization, and iron hydroxides

by the alteration grade, with higher values corresponding to the most altered samples (Table 2).

The tailings' As concentrations were in the range of 260–5,900 mg/kg, with RD-3 and RD-4 (Figs. 2d and 3; Table 2) being the samples with the highest As concentrations. High-intensity rain events during the summer season and steep slopes facilitate fluvial transport of tailing particles downstream of the drainage network. This transport mechanism has been active since the beginning of the mining activities in the last century.

The As concentration in the sediment samples were in the range of 9–164 mg/kg (Fig. 3; Table 2). The samples with the higher concentrations were located downstream of the intrusive body, with sample SED-1 being the one with the highest concentration (Fig. 3). This sample showed colors ranging from beige to brown, indicating that the sample was mainly composed of debris derived from the mineralized area. The As concentrations decrease with increasing distance from the intrusive body (Fig. 3; Table 2). The As concentrations in the soil samples were in the range of 10.8–373 mg/kg (Fig. 3; Table 2). Two-thirds of the soil samples were taken from agricultural areas and one-third from grazing land. The highest concentrations were found in the southern part of the GP (Fig. 3), at a flooding area (pond) close to a doline. The results indicate that the sediments derived from the intrusive body and the old mining tailings are the primary As source in the study area. Depositions in and around dolines at the southern fringe are a secondary source of As to groundwater.

Water samples

The groundwater quality was assessed according to the Mexican and the World Health Organization drinking water guidelines (WHO 2022; NOM-127-SSA1-1994 n.d.; Table 1).

Physicochemical parameters

Groundwater samples from the study area ($n = 92$ samples) showed temperatures varying from 14.9 to 29.9 °C (average $T = 22.6$ °C). The springs located in the limestone ranges show the lower temperatures; in contrast, the higher temperatures are located in the wells in the southern section of the study area tapping the Guaxcama Formation. The pH values ranged from 6.4–8.2 (average 7.2), indicating circum-neutral conditions in the shallow aquifers. Electrical conductivity values ranged from 180 to 4,770 µS/cm (average 1,307 µS/cm). The higher values of EC are found in the deep wells tapping the sulfate-rich Guaxcama Formation. In addition, these high values follow the general direction of groundwater flow. On the other hand, the lower EC values are found in the springs located in the mountain ranges around the CB, indicating recent infiltration.

Major ions

The major ions show a heterogeneous distribution in the study area (Table 1). The HCO_3^- concentration varies from 106 to 658 mg/L (average 338 mg/L) showing the influence of the limestone units. Cl^- concentrations were 9.1–690 mg/L (average 60.6 mg/L) with highest values in the deep wells near Cerritos, indicating deep groundwater circulation. SO_4^{2-} values vary from 1 to 1,964 mg/L (average 412 mg/L) and are mainly located in the deep and dug wells tapping the sulfate-rich Guaxcama Formation. NO_3^- concentration varies from 0.4 to 237 mg/L (average 24.7 mg/L), showing the influence of the intensive agricultural area near Villa Juarez. F^- values range from 0.01 to 2.2 mg/L (average 0.8 mg/L), and Na^+ ranges from 2 to 768 mg/L (average 80.4 mg/L), with the highest in samples from the deep wells near Cerritos. K^+ ranges from 0.6 to 29.1 mg/L (average 7.6 mg/L), with the highest mainly in the deep wells near Cerritos and to the south of Villa Juarez. Mg^{2+} concentrations range from 0.8 to 216 mg/L (average 40.6 mg/L), and Ca^{2+} ranges from 32.8 to 589 mg/L (average 169 mg/L). Most of the samples (45%) are of Ca–HCO_3 water type and 25% of Ca–SO_4 water type. The first water type is found in springs, dug wells, and deep wells tapping the limestone units, and the second water type is related to dug wells and deep wells tapping the gypsum units (Fig. 4). The remaining 30% of the water types vary from Na–HCO_3 (10%), Ca–Cl^- (1%), Na–Cl (1%), Na–SO_4 (3%), and unspecific mixtures (15%).

Arsenic spatial distribution

The As concentrations in groundwater range from 0.01 to 128 µg/L (Table 1), with the highest values located at the southern edge of the GP (Fig. 5). The sediments proceeding from the intrusive body are deposited at this location. A sample from the pond, used for livestock watering, shows the highest As concentration (226 µg/L) in the study area. The CB values above the WHO guideline were found in dug wells near Cerritos, as well as some dug and deep wells tapping the gypsum units in the southern section of the study area.

Low-As groundwater zones (<10 µg/L) were located mostly in the limestone units where springs, and dug and deep wells were located, indicating that the limestone does not contribute As to the groundwater. In total, 73% of the samples were within the As Mexican threshold; however, for the WHO guidelines, just 55% were within the threshold (Fig. 5), indicating a potential health hazard in the area. Furthermore, the species of As calculated using Geochemistry Workbench® were $HAsO_4^{2-}$ in 92% of the samples, $H_2AsO_4^-$ in 5% of the samples, and $As(OH)_3$ in 3% of the samples.

Isotopic values

Precipitation data are available from several meteorological stations within and around the study area, including one in Cerritos and one in the town of Guadalcazar; however, chemical or isotope data were not available. Calva (2011) characterized the stable environmental isotopes, $\delta^{18}O$ and $\delta^{2}H$, in precipitation for the San Luis Potosi state. Modern

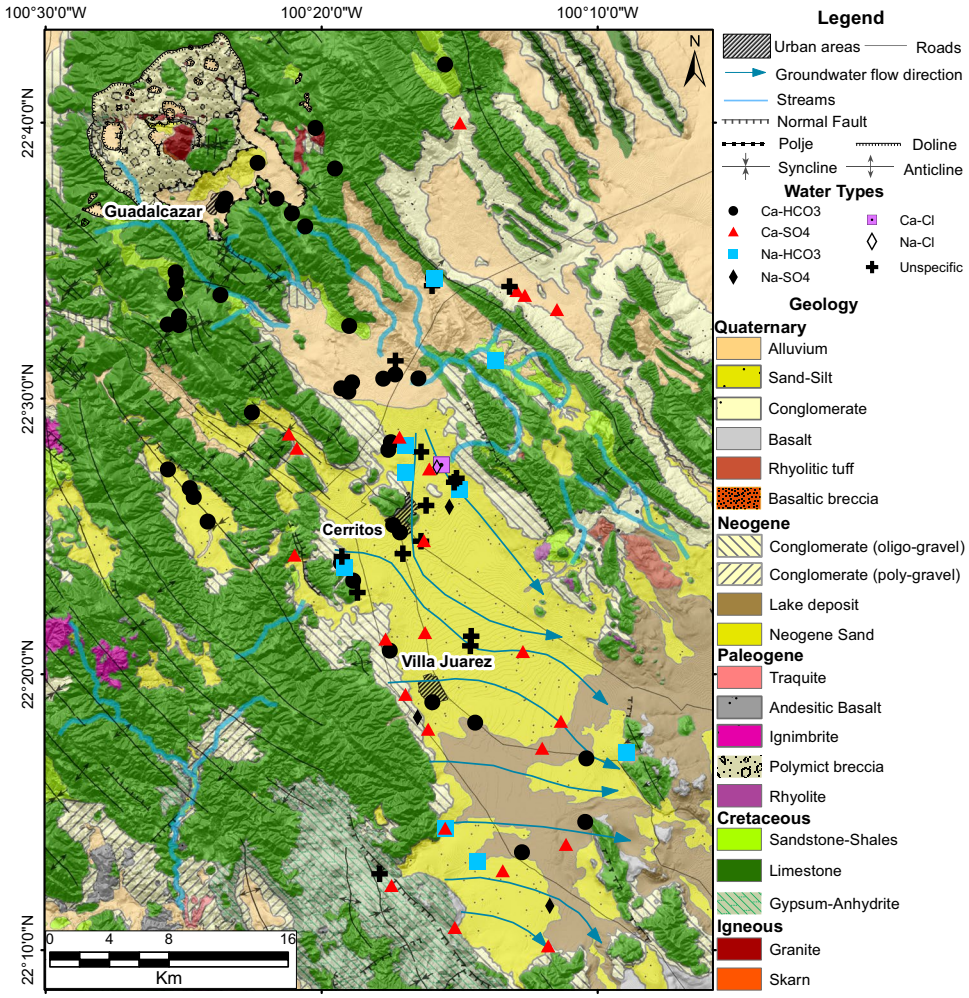

Fig. 4 Spatial distribution of the water types

rainfall from the region is presented by the Villa Juarez rain collector station (VJS), within the study area at an altitude of 1,165 masl (Fig. 1), where the range of composition for oxygen-18 ($\delta^{18}O$) and deuterium ($\delta^{2}H$) lies between –1.97 and –13.07‰ and –6.97 to –97.53‰, respectively, for the period between 2008 and 2010 (Calva 2011) with an average of –7.51 and –48.8‰, respectively. In addition, Calva (2011) reported isotopic ratios of precipitation in two locations (period 2008–2010), represented by the rain collector stations; the first (RCS-1) was located 50 km (2,634 masl) southwest and the second (RCS-2) was located 60 km (990 masl) southeast from Cerritos, respectively. The weighted average calculated for the total period of the sampling and for the rainy season for the sites are as follows: $\delta^{18}O$ –8.48, –8.43, –9.76, –9.85, –7.95, –8.44 and for $\delta^{2}H$ –56.72, –59.83, –63.79, –64.63, –51.90, –53.65, respectively (Fig. 6), which allows the identification of the main recharge area in the study area (Fig. 6). These three rain collector stations are in a representative position in the SMO and were used to determine the local meteoric water line (LMWL; Fig. 6) for the study area (n = 65) and will be used as a reference to elucidate the origin of the precipitation water sources. The Global Meteoric Water Line (GMWL) and the LMWL are widely used as references for interpreting the isotopic composition (e.g. Durowoju et al. 2019; Mathuthu et al. 2021; Stelling et al. 2021). The LMWL is similar to the GMWL with an equation of $\delta^{2}H = 8.098\delta^{18}O + 13.55$ and $R^2 = 0.9869$. The study area's LMWL slope (Fig. 6) is similar to the GMWL (Dansgaard 1964), while the isotopic composition of the groundwater samples plot on a line ($\delta^{2}H = 5.8534\delta^{18}O$ –9.176 and $R^2 = 0.9125$) with the slope being significantly lower than the LMWL and comparable to the theoretical slope of direct evaporation under conditions of 80% humidity (Clark and Fritz 1997), reflecting the influence of evaporation under relatively semiarid conditions. It also produces –10.12 $\delta^{18}O$ and –68.44 $\delta^{2}H$ values (Fig. 6), corresponding to the initial water obtained at an altitude of 2,634 masl.

The deuterium excess (d) value was defined as the intercept of the GMWL when the slope is 8 (Dansgaard 1964). This factor gives information on the physical conditions in the vapor source area and moisture recycling. It

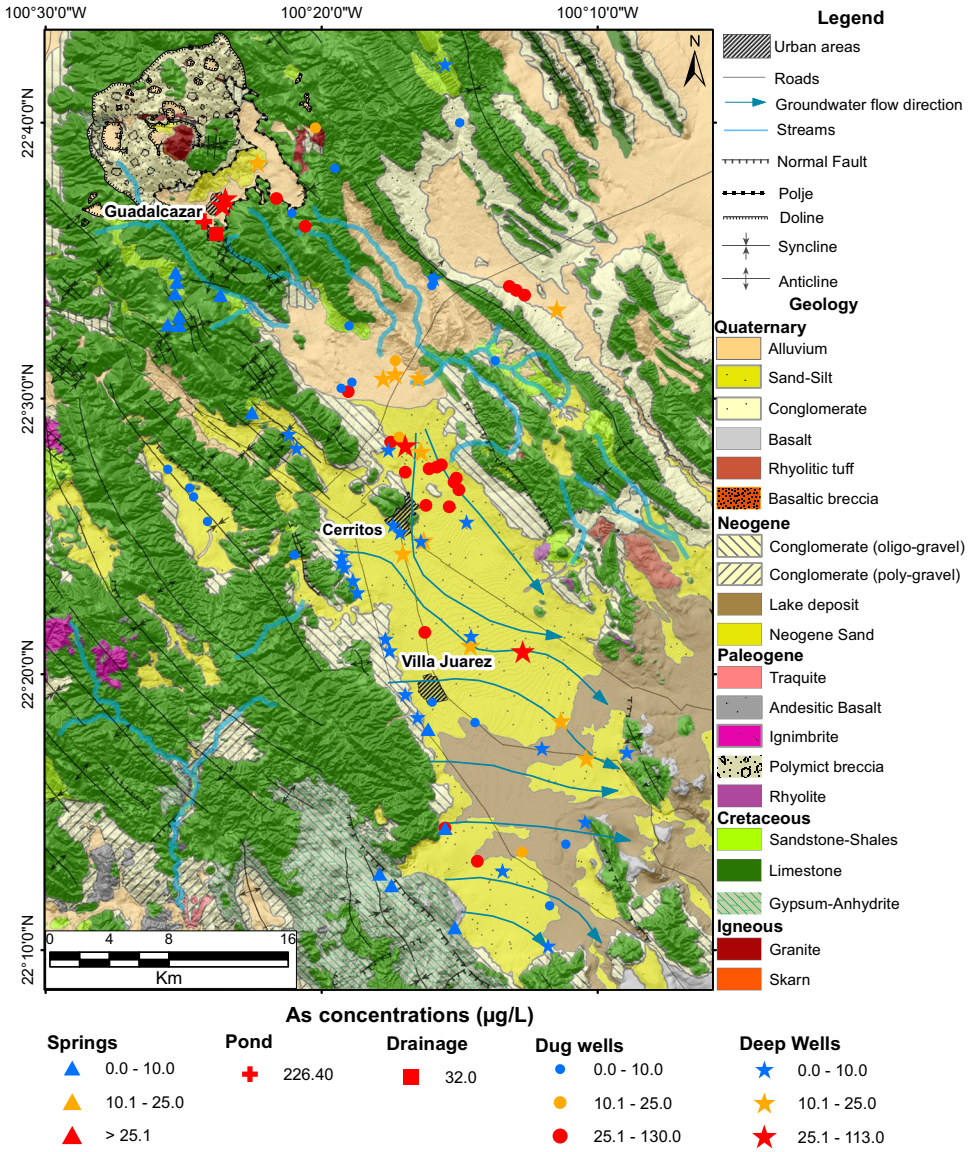

Fig. 5 Spatial arsenic distribution

is specifically sensitive to the conditions during the evaporation of water from the (ocean) surface, i.e. the moisture source conditions (Pfahl and Sodemann 2014). The *d* value for the LMWL is above 10‰, suggesting moisture recycling in the water source, in this case, the Gulf of Mexico. Considering the LMWL equation, the *d* values for groundwater samples vary widely, from 12.30 to 1.52‰, with a mean *d* value of 8.35‰. In general, these values are lower than 10‰, indicating groundwater recharge by summer seasonal precipitation from moisture circulation in a warm atmosphere.

The slope value of 5.8534 indicates a strong secondary evaporation (Clark and Fritz 1997; Qian et al. 2013, 2014) of the groundwater in the semiarid climate of the area under investigation. In particular, samples of dug wells in the range of –7.5 to –6 (%VSMOW) located to the northeast of CB showed elevated As concentrations varying from 20.6 to 103 µg/L, indicating an evaporation effect. Using the LMWL and Eq. (1), *d* was calculated in order to evaluate the evaporation effect in the study area.

$$d = \delta^2\mathrm{H} - 8.098\,\delta^{18}\mathrm{O} \quad (1)$$

Figure 7 shows three groups of dug wells, plotted depending on, for example, local conditions. Each group shows a good to excellent correlation of As concentrations and *d*. Group 1 is composed of three samples with excellent correlation ($R^2 = 0.98$). The sample with the highest *d* (5.62) and lowest As concentration (3.55 µg/L) is located in a basin fill valley between limestone ranges in the eastern part of Cerritos. The sample with the lowest *d* (1.52) and highest As concentration (51 µg/L) is located in the CB in the northern part of Villa Juarez.

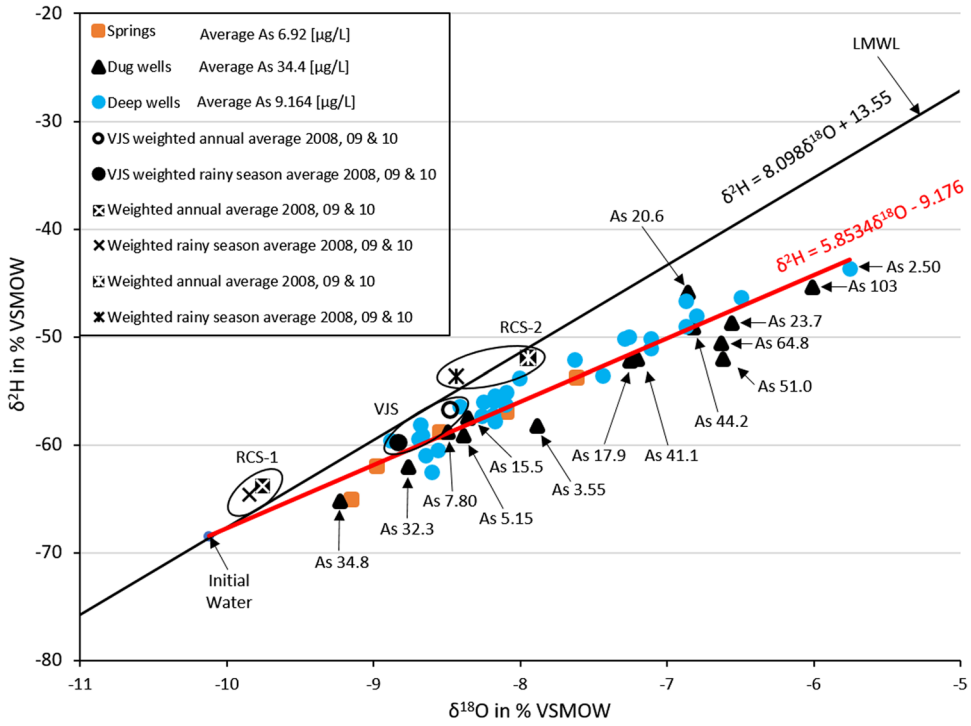

Fig. 6 Stable isotopes ($n = 47$) with the LMWL established for SLP region. Data for groundwater in the study area are diverting from the LMWL because of evaporation. As values of dug wells in µg/L

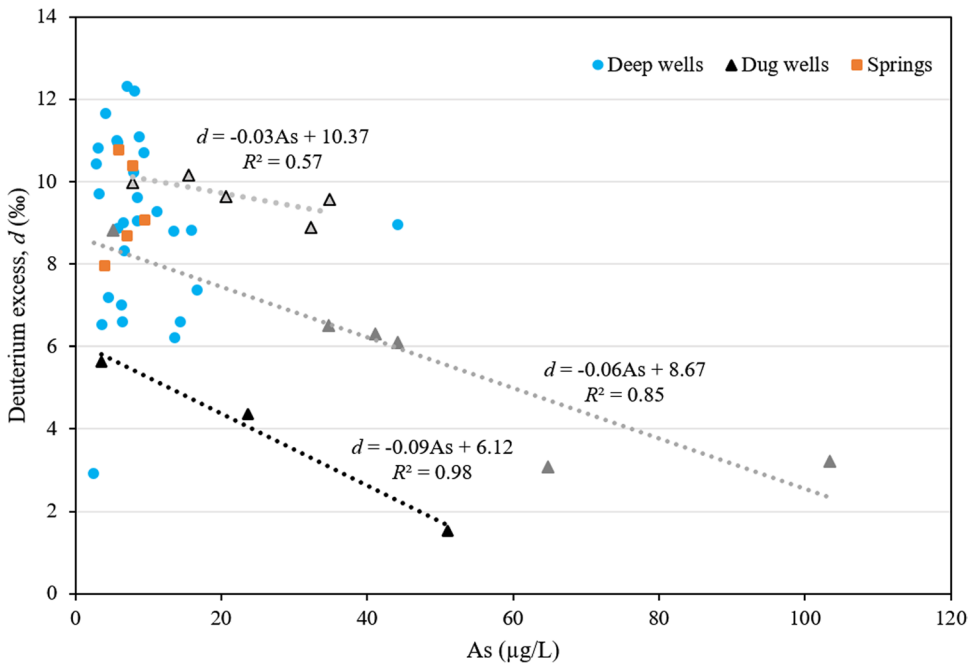

Fig. 7 Arsenic (As) concentration vs deuterium excess (d) ($n = 47$)

Group 2 is composed of six samples with a good correlation ($R^2 = 0.85$). The sample with the highest d (8.82) and lowest As concentration (5.15 µg/L) is located at the edge of Villa Juarez. The sample with the second lowest d (3.21) and highest As concentration (103 µg/L) is located in the northern part of Cerritos.

Group 3 is composed of five samples with a fair correlation ($R^2 = 0.57$). The sample with the highest d (9.97) and lowest As concentration (7.8 µg/L) is located to the southeast of Villa Juarez. The sample with the second lowest d (9.57) and highest As concentration (34.8 µg/L) is located in the northeast part

of Cerritos. As water from dug wells is not used for irrigation, there is no influence by isotopically shifted recharge from such a source. Furthermore, most of the plants in that section of CB do not have roots deep enough to influence the isotopic signature by transpiration. The data shown indicate that the evaporation of shallow groundwater contributes to an increase in As concentrations in the arid climate of the region.

Factor analysis

In principal axis factoring, an eigenvalue greater than 1 was set as a threshold for selecting the factors. The outcome was four factors (Table 3; Fig. 8), explaining 73% of the total variance in the chemical data. The rest of the factors explaining the cumulative variance (27%) appear not to have a clear relationship to the main factors controlling

Table 3 Total variance explained

Factor	Initial eigenvalues			Extraction sums of squared loadings			Rotation sums of squared loadings		
	Total	% variance	Cumulative %	Total	% variance	Cumulative %	Total	% variance	Cumulative %
Sulfate	4.217	35.145	35.145	4.025	33.541	33.541	3.555	29.628	29.628
Na–Cl	2.161	18.010	53.154	1.839	15.323	48.864	1.916	15.968	45.596
As–U	1.303	10.861	64.015	0.882	7.347	56.211	0.952	7.936	53.532
Nitrate	1.157	9.643	73.658	0.811	6.760	62.972	0.867	7.228	60.760

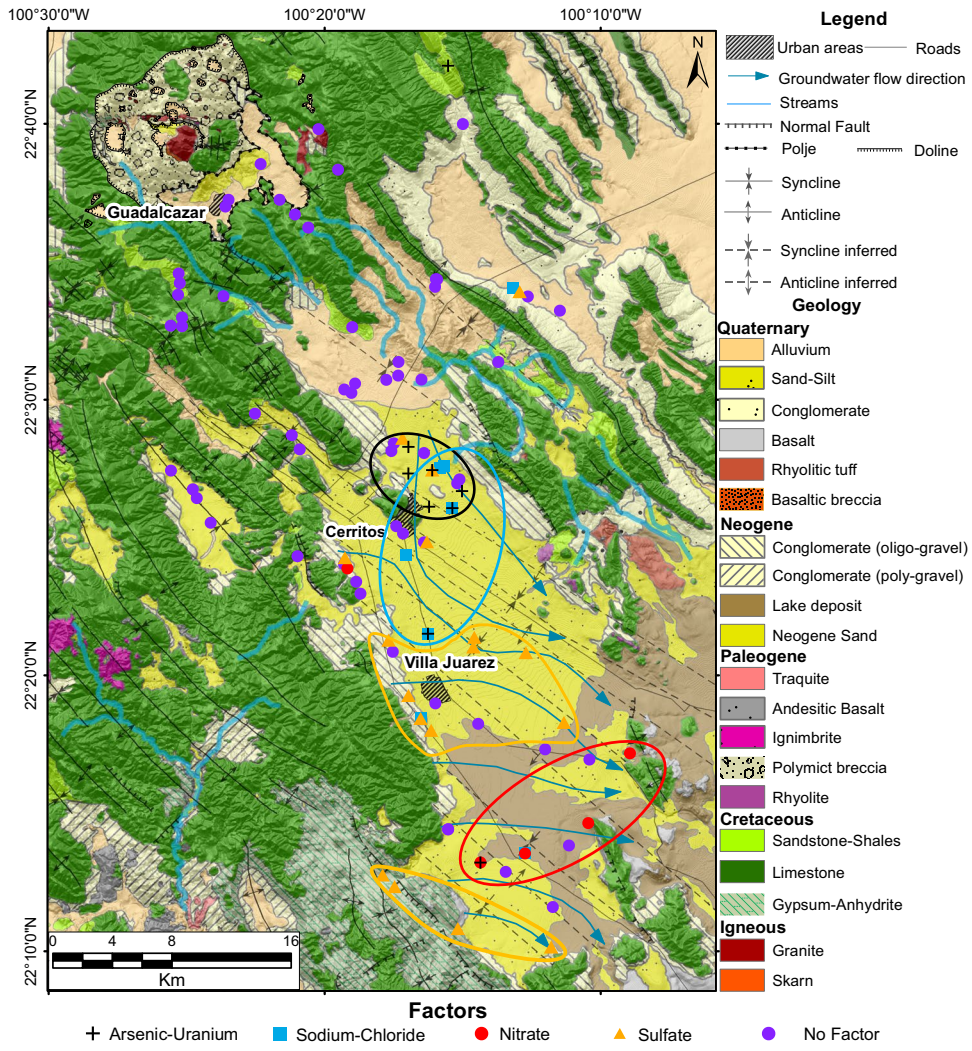

Fig. 8 Spatial factors distribution

the hydrochemical characteristics of the groundwater. In particular, bicarbonate, as the major ion in most of the samples, is not loading on a specific factor producing several factors with eigenvalues below 1, and these factors are not considered further. The presented results are based on the orthogonally rotated solution that explains 61% of the total variance. Table 4 shows the loading of the variables (elements) on each factor. Here, the interpretation of the factors is given. The first factor, denominated "sulfate", includes samples from the deep wells and dug wells tapping the Gypsum-Anhydrite formation in the south. The second factor is the "sodium-chloride" factor, which can be associated with deep groundwater. Samples related to this factor are located along the axes of anticlines and synclines conforming to the adjacent mountain ranges and projected to the area covered by the sediments of the CB (Fig. 8). The third factor is mainly defined by As and uranium. Samples from deep and dug wells tapping the basin fill are the main contributors (Fig. 8). As previously stated, the material from the mineralized zone contributes to As enrichment of the soils and sediments of this area, increasing the As concentrations of groundwater through lixiviation. In addition, the evaporation effect demonstrated with the isotopic results plays an important role in As concentrations. The fourth factor is the "nitrate" factor. This can be related to diffuse sources associated with intensive farming activities in greenhouses located in the area. Additionally, other natural processes include precipitation and decomposition of organic matter. Human activities include runoff from cultivated land, effluents from ponds and septic tanks, excessive nitrogen fertilizer application, deforestation, and change in soil organic matter due to crop rotation (Li et al. 2018, 2019; Molina et al. 2009). Finally, 59 samples did not have high scores on any of the four factors described, as indicated by the 39% unexplained variance. However, this unexplained variance ('no factor', Fig. 8) was plotted to show the spatial distribution. These samples are bicarbonate type and result from the dissolution of the limestones surrounding the basin without expressing special features in the principal axis factoring.

Table 4 Loadings of the variables: rotated factor matrix

Parameter	Factor			
	Sulfate	Na–Cl	As–U	Nitrate
Temp	0.37	0.10	–0.22	0.30
pH	–0.16	0.07	0.12	–0.38
EC	0.53	0.29	0.25	0.35
Na^+	0.13	0.78	0.28	0.12
K^+	0.19	0.46	0.22	0.28
Mg^{2+}	0.94	–0.05	0.02	–0.01
Ca^{2+}	0.80	0.02	–0.05	0.07
HCO_3^-	0.15	–0.07	0.40	0.19
Cl^-	0.06	0.93	–0.02	–0.09
SO_4^{2-}	0.93	0.12	0.09	0.03
NO_3^-	–0.18	0.17	0.09	0.57
Li	0.33	0.15	0.38	0.06
Sr	0.92	0.16	0.04	–0.01
Ba	–0.24	–0.15	0.00	–0.16
As	–0.14	0.24	0.76	–0.14
U	–0.09	0.19	0.90	–0.19

Discussion

Arsenic distribution in the solid samples

The solid samples showed high As concentrations around the intrusive body of El Realejo. These results are in accordance with the earlier study carried out in the area by the SGM (1998) and the results found by Casentini et al. (2010), Oyarzun et al. (2004), and Castro-Larragoitia (1995) under similar conditions as found in the study area. The highest As concentrations were found in the tailings from the old mining areas. These elevated concentrations are related to the enrichment of As from primary minerals in Fe hydroxides, as these minerals form important natural As sources and sinks (Nicolli et al. 1989, 2012; Smedley and Kinniburgh 2002; Matschullat 2000). Sediments transported by ephemeral streams that drain the El Realejo-Guadalcazar area are deposited in a pond at the southern fringe of the GP. As concentrations found in the topsoils of the pond were on average 189 mg/kg. In the Cerritos area, all the soil samples were above the reported mean background concentrations of As in continental crust and surface soils (Kabata-Pendias 2011). These As concentrations in soils indicate transport of fine material from the mineralized area into the CB, forming a secondary source of As to groundwater.

Arsenic distribution in the shallow groundwater and evaporation effect

Figure 5 shows groundwater from the shallow aquifer with heterogeneous distribution of As in the CB. Most of the sites contaminated with As were found in the central part of the study area. A spatial relationship was identified between the As concentrations and the general groundwater flow direction. Interpretation of the isotopic data allows the identification of the Guadalcazar mountain range as the main recharge area. Figure 6 allows the identification of the initial water (intercept) of the system. During the recharge process, part of the precipitation dissolves As from the solid matrixes. Likewise, the run-off associated with the process transports dissolved and suspended As to the GP. At this location, the surficial water in contact with soils and sediments rich in As again increases the As water concentrations and seeps

through sinkholes. From the southwest of the pond, wastewater from the town of Guadalcazar also flows into a water-filled doline draining into the limestone aquifer. This As-enriched wastewater (up to 32 µg/L) is another As source contributing to the shallow aquifers in the Cerritos Basin.

Based on the preceding, the general groundwater flow direction, the buried geological structures, and the As concentrations found in the center of the CB, a hydraulic connection was identified between the recharge area at CP and the As-enriched groundwater found in deep and dug wells tapping the basin fill sediments of CB. Additionally, the evaporation process increases the As concentrations in the shallow aquifer of the area (Fig. 6). Using the information generated in the hydrochemical analysis of *d* (Fig. 6), PHREEQC Version 3 code was used to evaluate the influence of evaporation in the As enrichment in a 20-step reaction. Since there are 55.55 moles of H_2O in 1 kg of water, the proposal was to evaporate in equal steps up to 95% of the 55.55 moles, to identify the concentration increase. These 20 steps were selected to get detailed information about As and Cl concentrations in the remaining water. In addition, two considerations were assumed to evaluate each group: (1) in the area there is no other source of chloride; (2) the lowest As concentration for each group was the initial concentration. This lowest concentration was located upstream of each group with reference to the groundwater flow direction. Figure 9a shows the results of group 1 in which the sample L-26 follows the expected As concentration; however, the sample L-08 presents more As than it should have, indicating evaporation and desorption effects. Figure 9b illustrates the results of group 2, where sample L-19 follows the expected As concentration; however, the adsorption process was presented in sample L-16 and the desorption process in samples 14-75, 14-142, and L-15. Figure 9c presents the results of group 3 in which none of the samples follow the expected As concentration, indicating further processes controlling As. However, similar to group 2, the adsorption process was identified in samples 14-144 and 14-164 and the desorption process in samples 14-40 and 14-168.

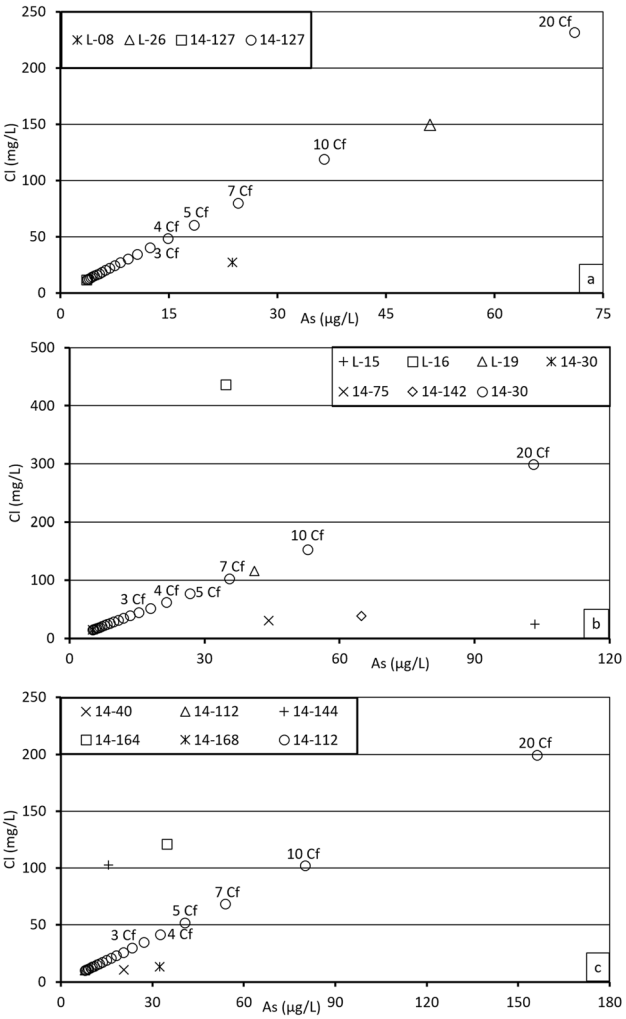

Fig. 9 Results of the modeling of evaporation in 20-step reaction for arsenic in **a** group 1, **b** group 2, and **c** group 3. Legend: Cf concentration factor

Statistical factors controlling As mobility

In the semiarid area, the factors controlling the As mobilization are "arsenic-uranium", "sulphate", "nitrate", and "sodium-chloride". The "arsenic-uranium" factor has a clear influence on samples from deep wells and dug wells tapping the basin fill (Fig. 8, black circle). At this location, the hydraulic connection between the recharge area and the GP has been identified. Water seeping through the material, from the mineralized zone deposited in the sinkholes, is getting enriched in As. Additionally, due to the aquifer shallowness in this area, evaporation increases the As concentrations, as the isotopic data show. The "sulphate" factor has influence in the deep wells and dug wells tapping the sulfate-rich Gypsum-Anhydrite Formation around and south of Villa Juarez. The "nitrate" factor is related to intense agriculture in the area and other natural and anthropogenic activities as previously described. Finally, the "sodium-chloride" factor is related to deep groundwater circulation in the study area, identified with the isotopic interpretation, the hydraulic connection, and by projected fold axes.

Conceptual model

The interpretation of the information generated and the conceptual model about sources and processes controlling As is explained in the cross-section shown in Fig. 10. The recharge area is located at the highest altitude of the study area with isotopic values of –10.12 $\delta^{18}O$ and 68.44 $\delta^{2}H$. In this recharge area, the precipitation infiltrates the igneous

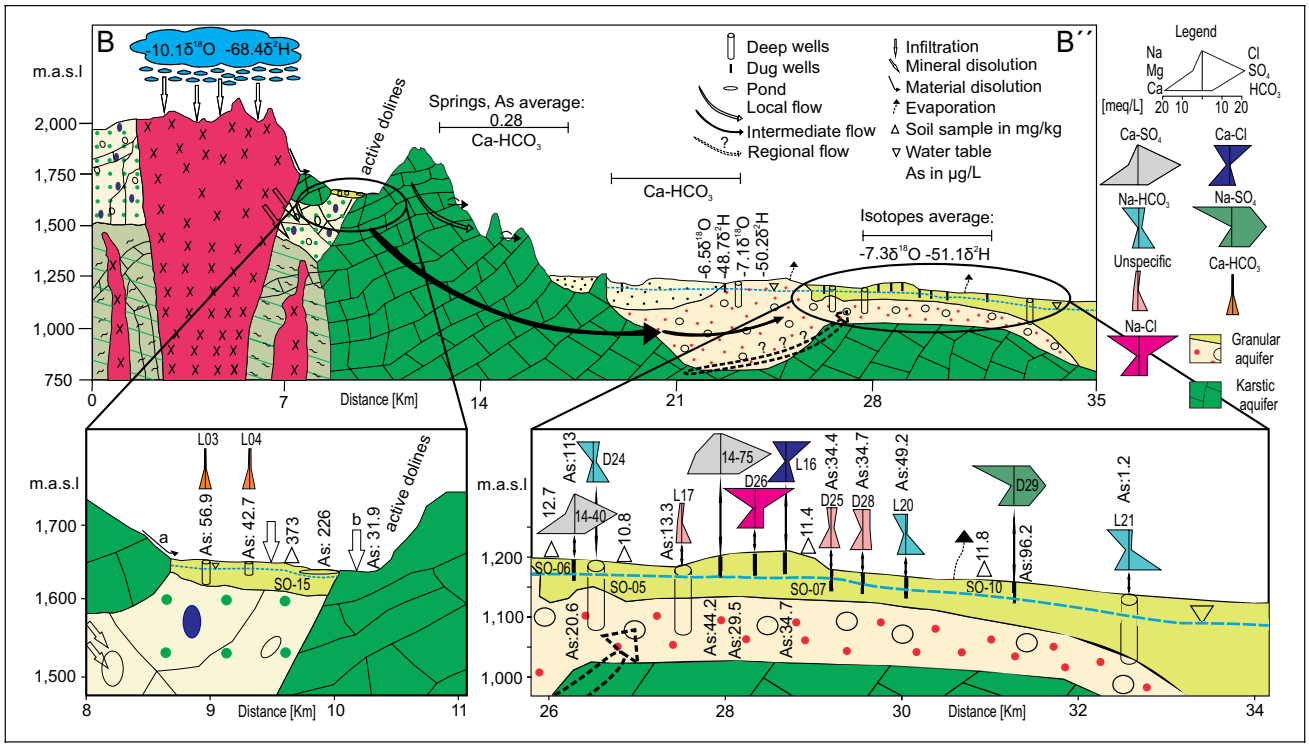

Fig. 10 Hydrogeological section B–B″. Legend: 'a' illustrates the path of the sediments derived from the mineralized area and 'b' shows the input of the doline to the karst system

rocks containing the As-loaded pyrites and produces groundwater with dissolved As that percolates the geological media as a primary source. In addition, mining residues distributed downstream of the intrusive body are a further primary source of As (marked "a" in Fig. 10). The run-off produced by the precipitation in contact with fluvial sediments derived from the intrusive body plays an important role in As enrichment as a secondary source. These fluvial sediments, with As concentration in the range of 152–664 mg/kg, are transported by ephemeral and intermittent streams and are deposited in depressions and sinkholes along the southern fringe of the GP where the pond is located. At this location, the surface water in contact with the soils with high As (189 mg/kg average) increases the As concentrations. This water enriched with As and also in contact with wastewater (As 32 µg/L) discharges in dolines located in the limestone that seeps into the karst system following the groundwater flow direction (marked "b" in Fig. 10). The As-enriched groundwater continues its flow through the karst system to the Cerritos Basin—there are no wells at the immediate northern border of the basin that would allow for sampling the inflow. Deep wells are low in As concentration when placed at the basin's rim and extracting groundwater from the surrounding limestone areas, but are high in As when placed in areas with inflow from the GP. Near Cerritos, the evaporation effect in the dug wells and soils with elevated As concentrations increase the As concentration in groundwater. In addition, sample D26 shows the inflow of regional groundwater of Na–Cl type mixing with the groundwaters in the basin. Finally, the As trace "vanishes" via the mixing of groundwaters from the GP with the inflow of bicarbonate waters from the limestone ranges around the basin and mixing to the south with Ca–SO_4 type waters from sediments of a former lake containing sulfates.

Conclusion

Calcareous rocks affected by a mineralized granitic intrusive body characterize the study area located in the physiographic entity of the Sierra Madre Oriental. This research addresses the comprehensive evaluation of the primary and secondary sources of As, not only in water, but also in solid samples, in order to identify the processes controlling its transport mechanism. The results of the solid samples showed high As concentrations exceeding the global background values. The water results showed the spatial distribution of As in the area and the factors controlling its mobility. The isotopic interpretation allowed the identification of the main recharge area and the role of the evaporation effect on As enrichment in the shallow aquifer. As primary sources are the sediments derived from the intrusive body and the tailings. The

secondary sources are the sediments derived from the intrusive body transported by ephemeral and intermittent streams that drain the El Realejo-Guadalcazar area and are deposited along the southern fringe of the Guadalcazar Polje. At this location, the As-enriched water seeps into a karst system that continues its path through the Cerritos Basin where the shallowness of the aquifer allows As enrichment due to the evaporation effect. In addition, the main As species is $HAsO_4^{2-}$ corresponding to oxic conditions in the shallow aquifer. Finally, understanding the behavior and transport of As in the study area can be used not only in Mexico, but also worldwide at sites with similar geological conditions.

Supplementary Information The online version contains supplementary material available at https://doi.org/10.1007/s10040-022-02562-w.

Acknowledgements We would like to acknowledge the Earth Science Department of the Engineering Faculty and the Geology Institute of the Autonomous University of San Luis Potosi, especially Dra. María Elena Garcia Arreola and Eng. Miguel Ángel Cortina Rangel for the ICP-MS and ICP-EOS measurements, and the Institute of Hydrogeology of the RWTH Aachen University, Germany, for supporting the field, laboratorial, and analytical work. Thanks as well to the Consejo Nacional de Ciencia y Tecnología (Conacyt) for scholarship No. 472208. Finally, we thank the anonymous reviewers for their valuable comments, which greatly improved our manuscript.

Funding Open Access funding enabled and organized by Projekt DEAL.

Declarations

Conflict of interest On behalf of all authors, the corresponding author states that there is no conflict of interest.

References

Ahmed KM, Bhattacharya P, Hasan MA, Akhter SH, Alam SMM, Bhuyian MAH, Imam MB, Khan AA, Sracek O (2004) Arsenic enrichment in groundwater of the alluvial aquifers in Bangladesh: an overview. Appl Geochem 19(2):181–200. https://doi.org/10.1016/j.apgeochem.2003.09.006

Alarcón-Herrera MT, Bundschuh J, Nath B, Nicolli HB, Gutierrez M, Reyes-Gomez VM, Nuñez D, Martín-Dominguez IR, Sracek O (2013) Co-occurrence of arsenic and fluoride in groundwater of semi-arid regions in Latin America: genesis, mobility and remediation. J Hazard Mater 262:960–969. https://doi.org/10.1016/j.jhazmat.2012.08.005

Alarcón-Herrera MT, Martín-Alarcón DA, Gutiérrez M, Reynoso-Cuevas L, Martín-Domínguez A, Olmos-Márquez MA, Bundschuh J (2020) Co-occurrence, possible origin, and health-risk assessment of arsenic and fluoride in drinking water sourcers in Mexico: geographical data visualization. Sci Total Environ 698:134168. https://doi.org/10.1016/jscitotenv.2019.134168

Banning A, Cardona A, Rüde TR (2012) Uranium and arsenic dynamics in volcano-sedimentary basins: an exemplary study in North-Central Mexico. Appl Geochem 27:2160–2172. https://doi.org/10.1016/j.apgeochem.2012.01.001

Biswas A, Majumder S, Neidhardt H, Halder D, Bhowmick S, Mukherjee-Goswami A, Kundu A, Saha D, Berner Z, Chatterjee D (2011) Groundwater chemistry and redox processes: depth dependent arsenic release mechanism. Appl Geochem 26:516–525. https://doi.org/10.1016/j.apgeochem.2011.01.010

Bundschuh J, Litter MI, Parvez F, Román-Ross G, Nicolli HB, Jean SH, Liu CW, López D, Armienta MA, Guilherme LRG, Gomez Cuevas A, Cornejo L, Cumbal L, Toujaguez R (2012) One century of arsenic exposure in Latin America: a review of history and occurrence from 14 countries. Sci Total Environ 429:2–35. https://doi.org/10.1016/j.scitotenv.2011.06.024

Calva D (2011) Caracterización isotópica de la precipitación en el Estado de San Luis Potosí [Isotopic characterization of precipitation in the State of San Luis Potosi]. MSc Thesis, Autonomous University of San Luis Potosi, Mexico

Casentini B, Pettine M, Millero FJ (2010) Release of arsenic from volcanic rocks through interactions with inorganic anions and organic ligands. Aquat Geochem 16:373–393. https://doi.org/10.1007/s10498-010-9090-3

Castro-Larragoitia J (1995) Environmental impacts of mining in the semi-arid area of Santa Maria de la Paz, Mexico. Karlsruher Geochem Hefte 9:1–156

Chakrabarti D, Singh SK, MdH R, Rahman MM (2018) Arsenic: occurrence in groundwater. In: Encyclopedia of environmental health, 2nd edn. Elsevier. https://doi.org/10.1016/B978-0-12-409548-9.10634-7

Chryssoulis S, Wilkinson N (1983) High silver content of fluid inclusions in quartz from Guadalcazar granite, San Luis Potosi, Mexico; a contribution to ore-genesis theory. Econ Geol 78(2):302–318. https://doi.org/10.2113/gsecongeo.78.2.302

Clark ID, Fritz P (1997) Groundwater. In: Clark ID, Fritz P (eds) Environmental isotopes in hydrogeology. CRC, New York

Comisión Nacional de Agua Dirección local en San Luis Potosí (CONAGUA) (2019) Información de Estaciones Meteorológicas de Cerritos y Guadalcázar [Weather station information for Cerritos and Guadalcázar]. CONAGUA, Mexico City

Dansgaard W (1964) Stable isotopes in precipitation. Tellus 16(4). https://doi.org/10.3402/tellusa.v16i4.8993

Durowoju O, Odiyo JO, Ekosse GIE (2019) Determination of isotopic composition of rainwater to generate local meteoric water line in Thohoyandou, Limpopo Province, South Africa. Water 45(2). https://doi.org/10.4314/wsa.v45i2.04

Gunderson L (1998) United States Geological Survey certificate of analysis granodiorite, Silver Plume, Colorado, GSP-2. US Geological Survey; Denver, CO

Guo H, Zhang B, Li Y, Berner Z, Tang X, Norra S, Stüben D (2011) Hydrogeological and biogeochemical constrains of arsenic mobilization in shallow aquifers from the Hetao basin, Inner Mongolia. Environ Pollut 159:876–883. https://doi.org/10.1016/j.envpol.2010.12.029

Guo H, Zhang Y, Xing L, Jia Y (2012) Spatial variation in arsenic and fluoride concentrations of shallow groundwater from the town

of Shahai in the Hetao basin, Inner Mongolia. Appl Geochem 27:2187–2196. https://doi.org/10.1016/j.apgeochem.2012.01.016

Guo H, Wen D, Liu Z, Jia Y, Guo Q (2014) A review of high arsenic groundwater in Mainland and Taiwan, China: distribution, characteristics and geochemical processes. Appl Geochem 41:196–217. https://doi.org/10.1016/j.apgeochem.2013.12.016

He X, Li P, Ji Y, Wang Y, Su Z, Elumalai V (2020) Groundwater arsenic and fluoride and associated arsenicosis and fluorosis in China: occurrence, distribution and management. Expo Health 12(3):355–368. https://doi.org/10.1007/s12403-020-00347-8

He X, Li P, Wu J, Wei M, Ren X, Wang D (2021) Poor groundwater quality and high potential health risks in the Datong Basin, northern China: research from published data. Environ Geochem Health 43(2):791–812. https://doi.org/10.1007/s10653-020-00520-7

Instituto Nacional de Estadística Geografía e Informática (INEGI) (2002) Estudio Hidrológico del Estado de San Luis Potosí, México [Hydrological study of the State of San Luis Potosi, Mexico]. https://www.inegi.org.mx/app/biblioteca/ficha.html?upc=702825224097. Accessed 29 May 2020

Instituto Nacional de Estadística Geografía e Informática (INEGI) 2020) Marco Geoestadistico Municipal 2020. http://www.cuentame.org.mx/monografias/informacion/slp/poblacion/default.aspx?tema=me&e=24. Accessed 02 Jul 2021

Kabata-Pendias A (2011) Trace elements in soils and plants, 4th edn. Taylor & Francis, London

Konefke LT (2018) Causes for elevated concentrations of arsenic and uranium in the northern Cerritos Basin, San Luis Potosí, México. MSc Thesis, RWTH Aachen University, Germany

Li P, He S, Yang N, Xiang G (2018) Groundwater quality assessment for domestic and agricultural purposes in Yan'an City, northwest China: implications to sustainable groundwater quality management on the Loess Plateau. Environ Earth Sci 77(23):775. https://doi.org/10.1007/s12665-018-7968-3

Li P, He X, Guo W (2019) Spatial groundwater quality and potential health risks due to nitrate ingestion through drinking water: a case study in Yan'an City on the Loess Plateau of northwest China. Hum Ecol Risk Assess 25(1–2):11–31. https://doi.org/10.1080/10807039.2018.1553612

Li Y, Li P, Cui X, He S (2021) Groundwater quality, health risk and major influencing factors in the lower Beiluo River watershed of northwest China. Hum Ecol Risk Assess 27(7):1987–2013. https://doi.org/10.1080/10807039.2021.1940834

López DL, Bundschuh J, Birkle P, Armienta MA, Cumbal L, Sracek O, Cornejo L, Ormachea M (2012) Arsenic in volcanic geothermal fluids of Latin America. Sci Total Environ 429:57–75. https://doi.org/10.1016/j.scitotenv.2011.08.043

Mackey EA, Christopher SJ, Long SE, Marlow AF, Murphy KE, Paul RL et al (2010) Certification of three NIST renewal soil standard reference materials for element content: SRM 2709a San Joaquin soil, SRM 2710a Montana soil I, and SRM 2711a Montana soil II. National Instit Standards Technol Spec Publ 260(172):1–39

Mathuthu J, Mokhine ND, Mkiva N, Nde SC, Dennis I, Hendriks J, Palamuleni L, Kupi TG, Mathuthu M (2021) Determining water isotope compositions for the IAEA WICO and NorthWest Villages, South Africa. Water 13:2801. https://doi.org/10.3390/w13202801

Matschullat J (2000) Arsenic in the geosphere: a review. Sci Total Environ 249(1–3):297–312. https://doi.org/10.1016/S0048-9697(99)00524-0

Meng X, Dupont RR, Sorensen DL, Jacobson AR, McLean JE (2017) Mineralogy and geochemistry affecting arsenic solubility in sediment profiles from the shallow basin-fill aquifer of Cache Valley Basin, Utah. Appl Geochem 77:126–141. https://doi.org/10.1016/j.apgeochem.2015.12.011

Molina M, Aburto F, Calderón R, Cazanga M, Escudey M (2009) Trace element composition of selected fertilizers used in Chile: phosphorus fertilizers as a source of long-term soil contamination. Soil Sediment Contam 18:497–511. https://doi.org/10.1080/15320380902962320

Morales I, Villanueva-Estrada RE, Rodríguez R, Armienta MA (2015) Geological, hydrogeological, and geothermal factors associated to the origin of arsenic, fluoride, and groundwater temperature in a volcanic environment "El Bajío Guanajuatense", Mexico. Environ Earth Sci 74:5403–5415. https://doi.org/10.1007/s12665-015-4554-9

Navarro O, González J, Júnez-Ferreira HE, Bautista CF, Cardona A (2017) Correlation of arsenic and fluoride in the groundwater for human consumption in a semiarid region of Mexico. Procedia Eng 186:333–340. https://doi.org/10.1016/j.proeng.2017.03.259

Nicolli HB, Suriano JM, Gómez Peral MA, Ferpozzi LH, Baleani OA (1989) Groundwater contamination with arsenic and other trace elements in an area of the Pampa, Province of Córdoba, Argentina. Environ Geol Water Sci 14(1):3–16. https://doi.org/10.1007/BF01740581

Nicolli HB, Bundschuh J, García JW, Falcón CM, Jean JS (2010) Sources and controls for the mobility of arsenic in oxidizing groundwaters from loess-type sediments in arid/semi-arid dry climates: evidence from the Chaco-Pampean plain (Argentina). Water Res 44:5589–5604. https://doi.org/10.1016/j.watres.2010.09.029

Nicolli HB, Bundschuh J, Blanco MC, Tujchneider OC, Panarello HO, Dapeña C, Rusansky JE (2012) Arsenic and associated trace-elements in groundwater from the Chaco-Pampean plain Argentina: results from 100 years of research. Sci Total Environ 429:36–56. https://doi.org/10.1016/j.scitotenv.2012.04.04

NOM-127-SSA1-1994 (n.d.) Diario Oficial de la Federación (DOF) [Official Gazette of the Federation (DOF)]. NORMA Oficial Mexicana, NOM-127-SSA1-1994, México, D.F. https://www.gob.mx/cms/uploads/attachment/file/110534/NOM_127_SSA1_1994.pdf,. Accessed 28 May 2020

Oyarzun R, Lillo J, Higueras P, Oyarzún J, Maturana H (2004) Strong arsenic enrichment in sediments from the Elqui watershed, northern Chile: industrial (gold mining at El Indio–Tambo district) vs. geologic processes. J Geochem Explor 84(2):53–63. https://doi.org/10.1016/j.gexplo.2004.03.002

Palm J (2008) Hydrogeological mapping of the Cerritos aquifer system focusing on chemical groundwater evolution. Diploma Mapping Thesis, RWTH Aachen University, Germany

Panagiotaras D, Nikolopoulos D (2015) Arsenic occurrence and fate in the environment: a geochemical perspective. Earth Sci Clim Change 6:269. https://doi.org/10.4172/2157-7617.1000269

Pfahl S, Sodemann H (2014) What controls deuterium excess in global precipitation? Clim Past 10:771–781. https://doi.org/10.5194/cp-10-771-2014

Podgorski J, Berg M (2020) Global threat of arsenic in groundwater. Science 368:845–850. https://doi.org/10.1126/science.aba1510

Qian H, Li P, Wu J, Zhou Y (2013) Isotopic characteristics of precipitation, surface and ground waters in the Yinchuan Plain, northwest China. Environ Earth Sci 70(1):57–70. https://doi.org/10.1007/s12665-012-2103-3

Qian H, Wu J, Zhou Y, Li P (2014) Stable oxygen and hydrogen isotopes as indicators of lake water recharge and evaporation in the lakes of the Yinchuan Plain. Hydrol Process 28:3554–3562. https://doi.org/10.1002/hyp.9915

Rodríguez-Hernández E, López-Doncel R, Barboza-Gudiño JR, Cruz-Márquez J (2009) Análisis sedimentológico-facial de clastos formadores de brechas calcáreas cretácicas de una zona transicional plataforma-cuenca en el centro de México [Sedimentological-facial analysis of Cretaceous limestone breccia forming clasts from a transitional platform-basin zone in central Mexico]. Rev Mex Cienc Geol 26(3):687–708 http://www.scielo.org.mx/scielo.php?script=sci_arttext&pid=S1026-87742009000300012. Accessed 29 May 2020

Rüde TR (1996) Beiträge zur Geochemie des Arsens [Contributions to arsenic geochemistry]. Karlsruher Geochemische Hefte 10:1–206
Schafmeister MT (1999) Geostatistics for hydrogeological practice. Springer, Heidelberg, Germany
Servicio Geológico Mexicano (SGM) (1998) Cartas Geológicas F14-4 [Geological map F14-4]. https://www.sgm.gob.mx/CartasDisponibles/. Accessed 29 May 2020
Servicio Geológico Mexicano (SGM) (2000) Cartas Geológicas F14-A65 [Geological map F14-A65]. https://www.sgm.gob.mx/CartasDisponibles/. Accessed 29 May 2020
Servicio Geológico Mexicano (SGM) (2008) Cartas Geológicas F14-A75, F14-A76, F14-A86 [Geological maps F14-A75, F14-A76, F14-A86]. https://www.sgm.gob.mx/CartasDisponibles/. Accessed 29 May 2020
Servicio Geológico Mexicano (SGM) (2010) Cartas Geológicas F14-A85 [Geological map F14-A85]. https://www.sgm.gob.mx/CartasDisponibles/. Accessed 29 May 2020
Smedley PL, Kinniburgh DG (2002) A review of the source, behaviour and distribution of arsenic in natural waters. Appl Geochem 17(5):517–568. https://doi.org/10.1016/S0883-2927(02)00018-5
Smedley PL, Kinniburgh DG (2013) Arsenic in groundwater and the environment. In: Selinus O (ed) Essentials of medical geology. Springer, Dordrecht, The Netherlands. https://doi.org/10.1007/978-94-007-4375-5_12
Sorg TJ, Chen ASC, Wang L (2014) Arsenic species in drinking water wells in the USA with high arsenic concentrations. Water Res 48:159–169. https://doi.org/10.1016/j.watres.2013.09.016
Soto Araiza RG, Argüelles Moreno JA, Torres Ramírez M (2007) Carta Geológico-Minera Cerritos F14-A76, Escala 1:50000 Estado de San Luis Potosí [Geological-mining chart Cerritos F14-A76, scale 1:50000 State of San Luis Potosí]. Mexicano Servicio Geológico, Mexico City
Srivastava S, Kumar Sharma Y (2013) Arsenic occurrence and accumulation in soil and water of eastern districts of Uttar Pradesh, India. Environ Monit Assess 185:4995–5002. https://doi.org/10.1007/s10661-012-2920-6
Stelling JM, Sebestyen SD, Griffiths NA, Mitchell CPJ, Green MB (2021) The stable isotopes of natural waters at the Marcell Experimental Forest. Hydrol Processes 35(10). https://doi.org/10.1002/hyp.14336
Torres-Hernández JR (1994) Evolución estructural de la Sierra de Guadalcázar, Estado de San Luis Potosí [Structural evolution of the Sierra de Guadalcázar, State of San Luis Potosí]. Master Thesis. Universidad Autónoma de México, México
Tristán-González M (1977) Cartografía Geológica, Hoja Buenavista, S.L.P. [Geological Mapping, Hoja Buenavista, S.L.P.]. Folleto técnico 54 Geología 14, Instituto de Geología, Universidad Autónoma de San Luis Potosí, México
USEPA (2004) Method 9045D: soil and waste PH. United States Environmental Protection Agency, 5 pp. https://www.epa.gov/dwstandardsregulations. Accessed 25 January 2022
Wang YY, Chai LY, Yang WC (2019) Arsenic distribution and pollution characteristics. In: Chai LY (ed) Arsenic pollution control in nonferrous metallurgy. Springer, Singapore. https://doi.org/10.1007/978-981-13-6721-2_1
Wei M, Wu J, Li W, Zhang Q, Su F, Wang Y (2021) Groundwater geochemistry and its impact on groundwater arsenic enrichment, variation, and health risks in Yongning county, Yinchuan Plain of Northwest China. Exposure Health. https://doi.org/10.1007/s12403-021-00391-y
WHO (2022) Guidelines for drinking-water quality, 4th edn. incorporating the first and second addenda. World Health Organization. Geneva, Switzerland
Zabala ME, Manzano M, Vives L (2016) Assessment of processes controlling the regional distribution of fluoride and arsenic in groundwater of the Pampeano Aquifer in the Del Azul Creek basin (Argentina). J Hydrol 541:1067–1087. https://doi.org/10.1016/j.jhydrol.2016.08.023
Zhu X, Wang R, Lu X, Liu H, Li J, Ouyang B, Lu J (2015) Secondary minerals of weathered orpiment-realgar-bearing tailings in Shimen carbonate-type realgar mine, Changde, central China. Miner Petrol 109:1–15. https://doi.org/10.1007/s00710-014-0344-4